

**ENHANCEMENT OF SUPERCONDUCTIVITY**

**IN**

**THIN ALUMINUM FILMS**

**ENHANCEMENT OF SUPERCONDUCTIVITY  
IN  
THIN ALUMINUM FILMS**

**By**

**OREST ALBERT EDWARD CHERNEY, B. Sc.**

**A Thesis**

**Submitted to the Faculty of Graduate Studies**

**in Partial Fulfilment of the Requirements**

**for the Degree**

**Master of Science**

**McMaster University**

**May 1969**

MASTER OF SCIENCE (1969)  
(Physics)

McMASTER UNIVERSITY  
Hamilton, Ontario

TITLE: Enhancement of Superconductivity in Thin Aluminum Films

AUTHOR: Orest Albert Edward Cherney, B.Sc.  
(University of Waterloo)

SUPERVISOR: Dr. J. Shewchun

NUMBER OF PAGES: viii, 51

SCOPE AND CONTENTS:

A description is given of a helium-3 system capable of reaching a temperature of 0.38° K and maintaining it for many hours. Temperature measurement is made by means of a germanium resistor, for which the calibration procedure is described.

The use of the helium-3 system is described in the investigation of the enhancement of the transition temperature,  $T_c$ , and the superconducting energy gap,  $\Delta(T)$ , of very thin aluminum films. The technique of constructing suitable tunneling junctions, as well as the electronics used in extracting this information, are also described.

The results of this investigation are discussed in relation to those in the literature, and proposed theories explaining the enhancement are discussed in the light of the present known experimental evidence.

## ABSTRACT

The phenomena of energy gap and transition temperature enhancement have been studied on very thin ( $35\text{-}80 \text{ \AA}$ ) aluminum films, using the technique of electron tunneling through a thin insulating barrier. Transition temperatures as high as  $2.16^\circ \text{K}$  have been measured, and the corresponding measured energy gaps are found to be unique. In addition, these thin superconducting films exhibit stable transition temperatures when held in a vacuum. However, upon breaking vacuum, oxide growth occurs, and the tunneling barrier becomes impenetrable. Existing theories proposed to explain the observed enhancements, are discussed in the light of present accumulated experimental evidence. However, it is found that none are capable of explaining adequately the observed enhancements.

## ACKNOWLEDGMENTS

The author wishes to express his gratitude for the encouragement and guidance from Dr. J. Shewchun, and to Dr. R. C. Dynes for suggesting this investigation and for his advice, without which, much time would have been lost. For a bursary, which made this investigation possible, the author is indebted to the National Research Council of Canada.

## TABLE OF CONTENTS

	Page No.
<b>Chapter I</b>	<b>INTRODUCTION</b>
1.1	Historical 1
1.2	Purpose of Thesis 3
<b>Chapter II</b>	<b>THEORY</b>
2.1	Introduction to BCS Theory of Superconductivity 4
2.2	BCS Ground State Energy 6
2.3	BCS Energy Gap 8
2.4	Electron Tunneling Between Superconductors 9
<b>Chapter III</b>	<b>APPARATUS AND TECHNIQUE</b>
3.1	Temperatures Below 1°K 13
3.2	Helium-3 Cryostat 13
3.3	Storage and Handling System for Helium-3 17
3.4	Procedure 18
3.5	Temperature Measurement and Calibration 20
3.6	Tunneling Sample Preparation 21

	Page No.
3.7 Current vs. Voltage Measurements	24
3.8 Derivatives of the I-V Characteristic	25
3.9 Transition Temperature Measurement	27
<b>Chapter IV</b>	
<b>EXPERIMENTAL RESULTS AND DISCUSSION</b>	
4.1 Thick Aluminum Films	29
4.2 Thin Aluminum Films	30
4.3 Summary of Results	31
<b>Chapter V</b>	
<b>MECHANISMS OF ENHANCEMENT OF <math>T_c</math></b>	
5.1 Quantization of Electronic Motion	33
5.2 Surface Enhancement	35
<b>Chapter VI</b>	
<b>CONCLUSIONS</b>	38
<b>ILLUSTRATIONS</b>	39
<b>BIBLIOGRAPHY</b>	50

## LIST OF ILLUSTRATIONS

		Page No.
Figure 1	Helium-3 Cryostat	39
Figure 2	Helium-3 Storage and Distribution System	40
Figure 3	Germanium Thermometer Calibration Curve (1.0 - 4.2°K)	41
Figure 4	Germanium Thermometer Calibration Curve (0.39 - 1.0°K)	42
Figure 5	Current vs. Voltage Measuring Circuit	43
Figure 6	Conductance vs. Voltage Measuring Circuit	44
Figure 7	Current vs. Voltage Curve of an Al-Al <sub>2</sub> O <sub>3</sub> -Pb Junction, approx. (100-20-1500 Å) thick	45
Figure 8	Conductance vs. Voltage Curve of Figure 7	46

Figure 9	Energy Gap vs. Temperature of an Al-Al <sub>2</sub> O <sub>3</sub> -Pb Junction, approx. (1500-20-1500 Å) thick	47
Figure 10	Energy Gap vs. Temperature for four Al-Al <sub>2</sub> O <sub>3</sub> -Pb Junctions, listed in Table 1	48
Table 1	Summary of Experimental Results	49

## I. INTRODUCTION

### 1.1 Historical

It has been known for some time that the weak coupling superconductors, consisting of very small crystallites ( $40-300 \text{ \AA}$ ), have anomalously high transition temperatures  $T_c$ , much higher than the bulk values.<sup>1</sup> Early work was conducted by Buckel and Hilsch (B6), and Khukhareva (K2). These investigators evaporated metal films onto glass substrates held at  $4.2^\circ\text{K}$ , obtaining films consisting of a system of very small crystallites with an enhanced transition temperature. Khukhareva (K2) investigated thin aluminum films of thicknesses ( $200-14000 \text{ \AA}$ ), obtaining films with enhanced transition temperatures as high as  $2.6^\circ\text{K}$ .

Both investigators found that upon warming the substrates to room temperature, the crystallites expanded, and, for sufficiently thin films, they became of the same dimensions as the film thickness. In addition, the enhanced transition temperatures returned to the normal values. It was thought that a decrease in the mean free path of the electrons, due to the system of very small crystallites, was a possible explanation for the observed enhancement.

More recently, it was found that the same metals exhibited enhanced transition temperatures when evaporated onto room temperature substrates, as

<sup>1</sup> The strong coupling superconductors Hg and Pb exhibit a decrease in  $T_c$  as the films are made thinner.

well as substrates held at 4.2°K (K1, A1, S2, C2). These films were prepared by admitting controlled amounts of oxygen into the evaporation system as the metals were being evaporated. High  $T_c$  films were also prepared without an external supply of oxygen, by evaporating from tungsten filaments with alumina inserts (A1, C2). The heated alumina provided an internal supply of oxygen. The observed increases in the  $T_c$ 's were of the same magnitude as those obtained by the early investigations (B5, K2). However, the films exhibited stable  $T_c$ 's upon storing at room temperature. It was also found that for a given oxygen pressure, variation of the film thickness did not produce any significant variation in either  $T_c$  or crystallite size. It was thought that these properties resulted from the precipitation of oxygen at the grain boundaries in the form of an oxide. The oxide prevented re-crystallization and grain growth, stabilizing  $T_c$  and formed Josephson junctions between the grains.

Superconductivity tunneling measurements by Walmsley, et al (W1) on very thin aluminum films (50-100 Å) revealed  $T_c$ 's as high as 2.25°K, of the same magnitude as those obtained previously, without the use of oxygen and onto substrates held at room temperature. Their measurements also revealed that the films exhibited unique energy gaps. It was thought that oxide, or other contamination, was no higher than the level found in thicker films which did not exhibit this enhancement. Furthermore, particle size, rather than associated intercrystallite impurities, seemed to be the necessary condition for producing the observed transition temperature enhancement.

## 1.2 Purpose of this Thesis

The purpose of this thesis is to substantiate to the experimental work of Walmsley, et al (W1), and to present new experimental data of energy gaps. Furthermore, it is shown that the evidence accumulated to date, suggests that these films are basically the same as those reported (A1, B6, C2, K2). Existing mechanisms of the enhancement are considered. However, it is found that none are satisfactory, and it is thought a new parameter, the volume density of crystallites, must enter into any proposed theory in explaining the enhancements.

## II. THEORY

### 2.1 Introduction to the BCS Theory of Superconductivity

The Bardeen, Cooper, Schrieffer theory (B2), hereafter referred to as the BCS theory of superconductivity, evolved from the observation of Cooper (C3), that if one considered two electrons excited slightly above the Fermi sea, they could form a real bound state, provided there was an attractive potential. Cooper showed that however small this attractive potential between two electrons above the Fermi sea, they lie within a region  $\approx k\Theta_D$  of the Fermi surface, where  $k$  is Boltzmann's constant, and  $\Theta_D$  is the Debye temperature. This bound state had its lowest energy if its net momentum was zero; that is, if the wave function was composed of a superposition of states in which the two electrons had equal and opposite momentum. The BCS theory provides a formalism for handling such a Cooper pair state for a microscopic number of such pair states.

In order that this theory work, one needs an attractive interaction between electrons, and it must be strong enough to overcome the repulsive screened Coulomb interaction. Bardeen and Pines (B3) showed that the effective matrix element for scattering of electrons with momentum  $\underline{k}$  and  $\underline{k}'$  by exchange of a phonon of momentum  $\underline{q}$  to new states  $(\underline{k} + \underline{q})$  and  $(\underline{k}' - \underline{q})$  could be written as (T2),

$$V_{kk'} = \frac{2\hbar\omega_q |M_q|^2}{(\epsilon_k - \epsilon_{k+q})^2 - (\hbar\omega_q)^2} \quad (1)$$

where  $\hbar\omega_q$  = phonon energy,

$\epsilon_k$  = electron energy measured from the Fermi surface,

and  $M_q$  = a matrix element for a single scattering by the electron-phonon coupling.

Expression (1) is negative if  $|\epsilon_k - \epsilon_{k+q}| < \hbar\omega_q \approx k\Theta_D$ .

Hence, in the region where Cooper pairs are formed, expression (1) will always have the negative sign and approximately equal to

$$V_{kk'} = - \frac{2|M_q|^2}{\hbar\omega_q} \quad (2)$$

That is, the interaction is an attractive one. To this electron-phonon term, the Coulomb repulsion term must be added. This term takes the form

$$\frac{4\pi e^2}{q^2} \mathcal{f} \quad (3)$$

where  $\mathcal{f}$  is the screening correction. An effective matrix element containing expressions (2) and (3) is defined by BCS as,

$$-V = \left\langle - \frac{2|M_q|^2}{\hbar\omega_q} + \frac{4\pi e^2}{q_{\text{eff}}^2} \right\rangle, \quad (4)$$

which is an average over those electron states which have  $|\epsilon_k| < \hbar\omega_q$ .

The BCS theory is based on the postulate that this effective matrix element (4) is negative, hence Cooper pairs are formed and superconductivity results.

## 2.2 BCS Ground State Energy

BCS calculate the ground state energy by considering the reduced problem in which the states are occupied in pairs, such that if  $k\uparrow$  is occupied, so is  $-k\downarrow$ . The ground state energy of a superconductor is then due to the correlation of these Cooper pairs of opposite spin and momentum and the screened Coulomb energy. The matrix element for transforming a pair in the state  $(\underline{k}\uparrow, -\underline{k}\downarrow)$  into the state  $(\underline{k}'\uparrow, -\underline{k}'\downarrow)$  can be written as

$$V_{kk'} = -2 \langle -\underline{k}'\downarrow, \underline{k}'\uparrow | H | -\underline{k}\downarrow, \underline{k}\uparrow \rangle, \quad (5)$$

where  $H$  is the reduced Hamiltonian, in which all common terms between the normal and superconducting states have been omitted. From (1) and (2), (5) is approximately a constant, so it is assumed that

$$\begin{aligned} \text{and} \quad V_{kk'} &\approx V, \text{ for } -\hbar\omega_q < \epsilon_k < \hbar\omega_q, \\ V_{kk'} &= 0, \text{ for } -\hbar\omega_q > \epsilon_k > \hbar\omega_q. \end{aligned} \quad (6)$$

If  $h_k$  is defined as the probability that the state  $(\underline{k}\uparrow, -\underline{k}\downarrow)$  is occupied, then the energy of the superconducting ground state, compared to the normal ground state at  $0^\circ\text{K}$  is

$$W(0) = \sum_{\underline{k}} 2 \epsilon_k h_k - \sum_{\underline{k}\underline{k}'} V_{kk'} \{ h_k (1 - h_{k'}) h_{k'} (1 - h_k) \}^{1/2}. \quad (7)$$

Applying the conditions of (6) to (7),

$$W(0) = \sum_{\underline{k}} 2 \epsilon_k h_k - V \sum_{\underline{k}\underline{k}'} \{ h_k (1 - h_{k'}) h_{k'} (1 - h_k) \}^{1/2}. \quad (8)$$

The first term of equation (8) expresses the energy difference of the system in the superconducting and normal states at  $0^\circ\text{K}$ . The larger second term,

gives the correlation energy for all possible transitions from the state  $(\underline{k}\uparrow, -\underline{k}\downarrow)$  to  $(\underline{k}'\uparrow, -\underline{k}'\downarrow)$ .

For the superconducting state,  $W(O)$  must be negative. Minimizing (8) with respect to  $h_k$  gives

$$h_k = 1/2 \left\{ 1 - \frac{\epsilon_k}{(\epsilon_k^2 + \Delta^2)^{1/2}} \right\}, \quad (9)$$

where 
$$\Delta = V \sum_{k'} \{h_{k'}(1 - h_{k'})\}^{1/2}, \quad (10)$$

the sum extending over states within the range  $|\epsilon_k| < \hbar\omega_q$ .

If (9) and (10) are combined, one obtains a condition on  $\Delta$ :

$$1/V = \sum_k \frac{1}{2(\epsilon_k^2 + \Delta^2)^{1/2}}. \quad (11)$$

Replacing the sum by an integral and recalling that  $V = 0$  for  $|\epsilon_k| > \hbar\omega_q$ , condition (11) is replaced by

$$1/N(O)V = \int_0^{\hbar\omega_q} \frac{d\epsilon}{(\epsilon^2 + \Delta^2)^{1/2}}. \quad (12)$$

where  $N(O)$  = density of states in the energy region considered and = constant.

Equation (12) has as a solution

$$\Delta = \frac{\hbar\omega_q}{\text{Sinh} \{1/N(O)V\}} \approx 2 \hbar\omega_q \exp \{-1/N(O)V\} \quad (13)$$

which, substituting into (8), gives the ground state energy at  $T = 0^{\circ}\text{K}$ ,

$$W(O) = - \frac{2N(O) (\hbar\omega_q)^2}{\exp \{2/N(O)V\} - 1}. \quad (14)$$

### 2.3 BCS Energy Gap

If  $f_{\mathbf{k}}$  is defined as the probability of occupation of  $\underline{k}\uparrow$  or  $-\underline{k}\downarrow$  by a single normal electron, and  $(1 - 2f_{\mathbf{k}})$  is the probability that neither  $\underline{k}\uparrow$  nor  $-\underline{k}\downarrow$  are occupied,  $W(T)$  will be equal to the sum of two terms; a kinetic energy term, and a correlation energy term. In terms of the Gibbs free energy function

$$G = W(T) - TS = W(T)_{KE} + W(T)_{CORR} - TS, \quad (15)$$

where  $W(T)_{KE} = 2 \sum_{\mathbf{k}} \epsilon_{\mathbf{k}} \{f_{\mathbf{k}} + (1 - 2f_{\mathbf{k}}) h_{\mathbf{k}}\}$

and  $W(T)_{CORR} = -V \sum_{\mathbf{k}\mathbf{k}'} \{h_{\mathbf{k}}(1 - h_{\mathbf{k}'})h_{\mathbf{k}'}(1 - h_{\mathbf{k}})\}^{1/2} \{(1 - 2f_{\mathbf{k}})(1 - 2f_{\mathbf{k}'})\}$

the second curly bracket assures that the correlated states are not occupied by normal electrons.

Through a similar analysis as before, one obtains an expression for the energy gap

$$\Delta(T) = V \sum_{\mathbf{k}} \{h_{\mathbf{k}}(1 - h_{\mathbf{k}'})\}^{1/2} (1 - 2f_{\mathbf{k}'}) . \quad (16)$$

Minimizing (15) with respect to  $f_{\mathbf{k}}$ , we obtain

$$f_{\mathbf{k}} = \left[ \exp \left\{ \left( \epsilon_{\mathbf{k}}^2 + \Delta^2(T) \right) / kT + 1 \right\} \right]^{-1} \quad (17)$$

The condition determining the energy gap (16) becomes

$$1/N(0)V = \int_0^{\hbar\omega_q} \frac{\tanh \left\{ \left( \epsilon^2 + \Delta^2(T) \right)^{1/2} / 2kT \right\} d\epsilon}{\left( \epsilon^2 + \Delta^2(T) \right)^{1/2}} , \quad (18)$$

where the sum has been replaced by an integral as before,  $f_{\mathbf{k}}$  replaced by (17) and using the fact that the distribution functions are symmetric in holes and electrons with respect to the Fermi energy. The transition temperature,  $T_c$ , is defined as the boundary of the region beyond which there is no real, positive  $\Delta$  which satisfies (18). Above  $T_c$ , therefore,  $\Delta = 0$  and the metal returns to the normal state. Below  $T_c$  the solution of (18),  $\Delta \neq 0$ , minimizes the free energy and we have the superconducting phase. To find the critical temperature  $T_c$ ,  $\Delta = 0$  is, therefore, substituted into (18) hence,

$$1/N(O)V = \int_0^{\hbar\omega_q} \frac{\tanh(\epsilon/2kT_c) d\epsilon}{\epsilon}$$

$$\text{or } kT_c = 1.14 \hbar\omega_q \exp\{-1/N(O)V\} \quad (19)$$

as long as  $kT_c \ll \hbar\omega_q$ , which corresponds to the weak coupling limit. Expressions (13) and (19) give  $2\Delta(O) = 3.52 kT_c$ . This ratio is predicted to be the same for all superconductors in the weak coupling limit.

#### 2.4 Electron Tunneling between Superconductors

The central part of the BCS theory of superconductivity is the creation of an energy gap in the electron density of states when a metal is made superconducting. Experimental evidence for this gap can be obtained by several different methods, but a particularly illustrative and simple one is by electron tunneling. In a tunneling experiment, the sample consists of a thin insulating layer, sandwiched between two evaporated metal films. Experimentally, the electron tunneling current through the insulating layer is observed as a function

of voltage applied between the two metal films. The tunneling experiment can be explained qualitatively by using a very simple model proposed by Giaever (G1). The interpretation of the experiment hinges on the assumption that the transition probability is proportional to the density of states in a superconductor. This assumption has been shown to be plausible by Bardeen (B1).

The "semiconductor model" for the superconducting sandwich consists of a BCS density of states function for each of the two superconductors separated by an insulator. When no potential is applied across the barrier, the two Fermi levels will line up at the same energy. The application of a potential  $V$  will cause the Fermi level of one metal to shift an energy  $eV$  with respect to the other.

The transition probability of tunneling from an occupied state in film 1, to an unoccupied state in film 2, can be written as

$$P_{12} = \frac{2\pi}{\hbar} |M_{12}|^2 N_2(E) (1 - f_2(E)) \quad (20)$$

where  $N_2(E)$  = density of states in film 2,

$f_2(E)$  = Fermi function,

and  $M_{12}$  = transition matrix connecting the two states.

Consequently, the total current tunneling from film 1 to film 2 is the sum of all these transitions,

$$I_{12} = N_1(0) N_2(0) \frac{2\pi e}{\hbar} \int_{-\infty}^{\infty} |M_{12}|^2 f_2(E - eV) f_1(E) (1 - f(E - eV)) f(E) dE \quad (21)$$

where  $f(E)$ , the reduced density of states has been defined as

$$f(E) = N(E) / N(0)$$

and  $N(0)$  = density of states in the normal metal.

Similarly, the current tunneling from film 2 to film 1,

$$I_{21} = N_1(O) N_2(O) \frac{2\pi e}{\hbar} \int_{-\infty}^{\infty} |M_{21}|^2 f_2(E - eV) f_1(E) (1 - f(E)) f(E - eV) dE \quad (22)$$

and, assuming  $|M_{12}|^2 = |M_{21}|^2$ , the total current tunneling through the insulating barrier can be written as

$$I = N_1(O) N_2(O) \frac{2\pi e}{\hbar} \int_{-\infty}^{\infty} |M_{21}|^2 f_2(E - eV) f_1(E) (f(E - eV) - f(E)) dE \quad (23)$$

We consider the case in which both films are superconducting, and it is assumed that  $|M_{12}|^2$  is a constant over the range considered, hence the current becomes

$$I = \frac{\sigma_n}{e} \int_{-\infty}^{\infty} f_1(E) f_2(E - eV) (f(E - eV) - f(E)) dE \quad (24)$$

where  $\sigma_n = \frac{2\pi e^2}{\hbar} N_1(O) N_2(O) |M_{12}|^2$

and is approximately a constant. It is clear that the tunneling current is dependent upon the relative positions of the density of states functions.

As a specific example, consider the experimental current-voltage characteristic of an Al - Al<sub>2</sub>O<sub>3</sub> - Pb junction, as illustrated in figure 7. On the basis of the simple model proposed by Giaever (G1), this I - V curve exhibits almost negligible current flow as expected at 1.07°K, until the voltage corresponding to the energy  $\Delta_{Pb} - \Delta_{Al}$  is applied. This negligible current flow is due to thermal excitations. When the voltage is increased further, the same number of electrons tunnel, hence the current decreases. Finally, when the voltage approaches the energy  $\Delta_{Pb} + \Delta_{Al}$ , the current will increase rapidly, breaking at a point and increases proportionally to the applied voltage.

At the voltages corresponding to the energies  $\Delta_{\text{Pb}} - \Delta_{\text{Al}}$  and  $\Delta_{\text{Pb}} + \Delta_{\text{Al}}$ , the BCS theory predicts a discontinuous rise at  $T = 0^\circ \text{K}$ . At finite temperatures, there is no discontinuous jump at these energies, and a certain amount of ambiguity is introduced in selecting the voltage corresponding to  $\Delta_{\text{Pb}} + \Delta_{\text{Al}}$  and  $\Delta_{\text{Pb}} - \Delta_{\text{Al}}$ . It is assumed that the point at which the slope of the I - V characteristic passes through a maximum indicates the energy gap  $\Delta_{\text{Pb}} + \Delta_{\text{Al}}$ , and the point of maximum slope in the negative resistance region indicates  $\Delta_{\text{Pb}} - \Delta_{\text{Al}}$ . Effectively, this corresponds to the point where, for an incremental change in voltage  $\Delta V$ , there is a maximum number of available states, into which tunneling can occur. Consequently, a plot of the conductance vs. voltage would be a more helpful aid in determining the values of  $\Delta_{\text{Pb}}$  and  $\Delta_{\text{Al}}$ . The experimental conductance vs. voltage plot of figure 7 is illustrated in figure 8. One can readily see that the points of maximum slopes are very easy to discern.

### III. APPARATUS AND TECHNIQUE

#### 3.1 Temperatures Below 1° K

The most direct method of obtaining temperatures below 1° K is by pumping on normal liquid helium. However, it is somewhat difficult to obtain temperatures well below 1° K by this technique, and the lower limit appears to be about 0.73° K (R1). Considerably lower temperatures can, however, be reached by the use of the light helium isotope, helium-3, as a refrigerant.

Liquid helium-3 has a normal boiling point of 3.195° K, and at all temperatures its vapor pressure is higher than that of normal liquid helium. Consequently, if the pressure is reduced, one obtains lower temperatures with helium-3, than with normal helium. Helium-3 does not undergo a phase transition, like that of helium-4 at the lambda-point, but remains a normal liquid down to very low temperatures, at least down to 0.008° K (Z1). There is, therefore, no film flow transporting fluid and heat; hence, liquid helium-3 can be pumped to much lower pressures than liquid helium-4. These two factors enable one to obtain temperatures below 0.5° K with a quite simple apparatus.

#### 3.2 Helium-3 Cryostat

The cryostat used is as illustrated in figure 1. The small stainless steel pot (1" dia. x 1" length) is the liquid helium-3 container, the bottom of

which is fitted with a 1/4" thick copper plate with 1/16" dia. holes drilled to a 1/8" depth. These holes increase the surface area of contact with the liquid helium-3, and insures good thermal contact with the germanium thermometer and sample mounted on the under side. Two thin wall stainless steel lines are silver soldered to the pot which is suspended 5 cm. within the outer stainless steel exchange gas chamber (1 3/4" dia. x 4 1/2" length). The centre 3/16" dia. line is used to pump on the liquid helium-3 and the other, a 1/16" dia. line coiled above the chamber is the liquid helium-3 fill line. The fill line connects to a 1/8" dia. stainless steel line which extends to the top of the cryostat. The centre line, as well as the 3/16" dia. stainless steel line used in evacuating the exchange gas chamber, are connected to radiation traps constructed from 1/2" copper pipe tees and elbows. These radiation traps are silver soldered to 1/2" dia. stainless steel lines, which extend to the top of the cryostat. In addition to these radiation traps, three copper fins, which extend to one half the diameter of the helium-3 pumping line, are inserted directly above the radiation trap. These fins aid in reducing the radiation entering the helium-3 pot. This trap offers little resistance to the gas flow, because it is suspended in a bath of helium at 1°K, where the gas density is high. Also, since the exchange gas pumping line is directly above the helium-3 pot, another radiation trap has been introduced to prevent radiation, which passes through the tee-elbow arrangement from striking the helium-3 pot.

Ten number 40 enameled copper wires, which are connected to the kovar seal at the top of the exchange gas chamber pumping line, pass down

this line into the exchange gas chamber and spiral around the helium-3 pot to the bottom, and are attached to the sample and germanium thermometer.

The exchange gas chamber is removable, so that samples can be mounted on the helium-3 pot, and sealed by an O-ring made from standard grade indium wire. This O-ring is usually replaced each time the exchange gas chamber is removed; however, if carefully removed, it will hold for three to four runs without lambda leaks developing.

Surrounding the entire assembly described in the preceding paragraph, are two dewars. The innermost dewar contains normal liquid helium pumped on by a 2000 liter/min. pump, such that the inner assembly is suspended in a bath at about 1°K. The outermost dewar contains liquid nitrogen. The entire cryostat is rigidly supported to the laboratory wall and floor, and separated from the pumping and distribution system by bellows.

When the pressure of the helium-3 vapor in the pot is reduced, the temperature, which the liquid helium-3 attains, is such that the rate of heat removal by evaporation, equals the rate of heat influx. The lowest temperature attained in this cryostat was 0.38°K, with the helium-3 bath temperature at 1.07°K. At this temperature, the recovery rate of the helium-3 gas was approximately determined, and using the known heat of evaporation (H1), the heat leak was estimated to be in the order of 75 ergs/sec. This heat leak is primarily due to radiation entering through the helium-3 pumping line.

The ten electrical leads, made of enameled number 40 copper wire, are thermally grounded on the exchange gas chamber at 1.07°K. It is reasonable to

assume that the heat conducted by these leads, would be dissipated in the helium-4 bath. The remaining length, about 15 cm., spiraled around the helium-3 pot, contributes at most 2 - 3 ergs/sec.

The production of heat by mechanical vibration cannot be estimated, and is reduced as much as possible by connecting the pumping lines with bellows, which dampen the vibrations.

The heat leak through the residual helium-4 gas in the exchange gas chamber can be neglected (S1) since the helium-4 exchange gas is pumped from the vacuum space at  $4.2^{\circ}\text{K}$  and then the outer and inner chambers are cooled to  $1.07^{\circ}\text{K}$  and  $0.38^{\circ}\text{K}$  respectively; hence, almost all the gas remaining in the exchange gas chamber is adsorbed on the walls of the chamber.

The amount of heat that the helium-3 gas in the pumping line could possibly conduct to the helium-3 bath, is difficult to estimate. However, this quantity should be much less than the rate at which heat must be supplied to raise the temperature of the gas being pumped from the liquid, from  $0.38^{\circ}\text{K}$  to  $1.07^{\circ}\text{K}$ . This quantity is estimated at about 5 ergs/sec. from DeBoer's work (D1).

The contribution of the pumping lines to the heat leak is also difficult to estimate, because of the uncertainty in the thermal conductivity of the stainless steel used. The heat conducted from the top of the cryostat to the exchange gas chamber can certainly be neglected, since this heat is absorbed by the helium-4 bath. Hence, the only contribution to the heat leak is from the two lines which connect to the helium-3 pot. Extrapolating the published thermal

conductivity data (P2) below  $1^{\circ}\text{K}$ , the heat conducted by these lines is estimated at between 10 - 20 ergs/sec. The remaining contribution to the heat leak is due to radiation entering through the helium-3 pumping line. This is reduced as much as possible by the illustrated radiation traps and fins in figure 1.

### 3.3 Storage and Handling System for Helium-3

Figure 2 illustrates the storage and handling system for the helium-3 cryostat. The system is completely portable and can be attached to other cryostats via O-ring connectors. The system consists of two sections: a helium-3 vacuum and storage system, and an auxiliary vacuum system.

The helium-3 vapor is pumped from the liquid with a Speedivac model 203B oil diffusion pump, that is backed by a Welch 1402 rotary pump, with a pumping speed of 140 liters/min. The pumping speed of the diffusion pump should be appreciably larger for helium, than the quoted value of 80 liters/sec. for air.

The exhaust side of the rotary pump is connected to three metal containers in which the helium-3 is stored when not in use. Each container stores approximately one liter of helium-3. Since the exhaust side of the rotary pump is not vacuum tight but oil tight, the pump is completely immersed in an oil bath to prevent leaks. A small leak in the system may, in fact, not be dangerous as the helium-3 is stored at a pressure which is always less than one atmosphere, and any air which enters will freeze out in the cryostat.

As is usually done with liquid coolants, the temperature of the helium-3

bath is varied by controlling the vapor pressure above the liquid. The pressure is adjusted by varying the pumping speed of the system by a needle valve, situated at the mouth of the diffusion pump.

The auxiliary vacuum system consists of a Speedivac model E02 oil diffusion pump, backed by a Welch Duo Seal model 1405B rotary pump. Initially, this system was used in evacuating and outgassing the helium-3 section through the valve F in figure 2 and, once outgassed, this valve was closed and never re-opened.

In an experiment, the auxiliary system is used initially to evacuate the helium-3 pot and the exchange gas chamber. Afterwards, it is used to remove the exchange gas and at the conclusion of the experiment when all the helium-3 has been returned, it is used to remove any air which may have been frozen out.

A cylinder of normal helium is connected to the auxiliary vacuum system for use as the exchange gas.

In both systems, the vacuum is monitored by a Speedivac IG-MA ionization gauge, as well as a Speedivac Pirani model M gauge. Both systems are capable of attaining a vacuum of  $5 \times 10^{-5}$  torr.

### 3.4. Procedure

The operation of the low temperature apparatus shown in figures 1 and 2 is straightforward and follows standard techniques. Initially, the outer dewar of figure 1 contains liquid nitrogen; valves A, B and C of figures 1 and 2 are open, and the helium-3 pot as well as the exchange gas chamber are evacuated. Once

a vacuum of about  $5 \times 10^{-5}$  torr is reached, valves A and C of figure 1 and A, B and C of figure 2 are closed, and the helium-3 gas from all three storage containers is then allowed into the cryostat down the helium-3 pumping line through valves E and D of figure 2 and valve B of figure 1. The inner dewar is then filled with liquid helium, and pumped upon, reaching a temperature of  $1.07^{\circ}$  K in about ten minutes. The helium-3 gas is condensed in the tee-elbow radiation trap, removed, and returned to the storage containers leaving any air which may have leaked into the system frozen inside the pumping line.

Helium-4 exchange gas is then allowed into the exchange gas pot, cooling the sample to  $1.07^{\circ}$  K. The helium-3 gas is allowed back into the cryostat through valve C of figure 1, condensing in the coiled section of the fill line and dripping into the pot. Once all of the helium-3 gas has condensed in the cryostat, the exchange gas chamber is evacuated, isolating the sample. The liquid helium-3 in the pot is then pumped through valve A of figures 1 and 2, reducing the temperature to  $0.38^{\circ}$  K. Approximately one liter of helium-3 gas is returned before this temperature is reached. Temperature control is achieved by adjusting the pumping speed with the needle valve, situated at the mouth of the helium-3 diffusion pump.

At the completion of the experiment, quick recovery of the helium-3 is achieved by filling the exchange gas chamber with exchange gas, and allowing the helium bath in the inner dewar to return to  $4.2^{\circ}$  K. All helium-3 lines up to valve E of figure 2, are evacuated, returning the helium-3 to their storage containers. The auxiliary vacuum system is then used in cleaning up the cryostat pumping lines.

### 3.5 Temperature Measurement and Calibration

The temperature was measured by means of a CryoCal germanium resistor. The resistance was measured by passing a  $1 \mu\text{A}$  current through the current leads of the resistor and the voltage developed across the voltage terminals was measured. The current and the voltage were monitored by Hewlett Packard Model 425A D.C. Micro-voltammeters. The resistor was thermally grounded by inserting it into a tightly fit thin brass sleeve, which was soldered to the bottom of the helium-3 pot. The resistance at the lowest temperature achieved was such that the heat leak into the helium-3 bath,  $4 \times 10^{-3}$  ergs/sec. was completely negligible. The germanium resistor was extremely sensitive at these low temperatures, and its temperature measurement remarkably reproducible upon recycling to room temperature.

The resistor was calibrated in the temperature range (0.39-4.2°K) by making use of the superconducting transition temperatures of six bulk superconductors, as well as the normal boiling point of liquid helium. All materials used were of high purity, better than 99.990 per cent, so the transition temperatures, which depend slightly on the purity, were extremely close to those published (W2).

The superconducting transition temperature was detected by using the change in magnetic properties which occurs at this temperature. On passing into the superconducting state, a metal becomes perfectly diamagnetic, excluding all magnetic flux. In a simple arrangement for detecting the transition temperature, two coils, each of about 200 turns of number 40 enameled copper

wire, were wound along the length of the material in the form of a rod about 2.0 cm. long and 2 mm. in dia., so that the material formed the core of a mutual inductance. A small alternating current at 1Khz. was passed through one of the coils, and the voltage induced in the other was amplified by a tuned 1Khz. amplifier, and fed into a PAR lock-in amplifier, the output of which was connected to the Y input of an X-Y recorder. The X input of the recorder plotted the resistance of the germanium resistor. When the material passes into the superconducting state, the coupling between the coils is greatly reduced, and the voltage across the secondary falls off to a small value. This point is extremely sharp, and provides a useful calibration point.

A function of the form  $R = cT^{-a}e^{b/T}$  was fitted in the temperature range (0.39-4.2° K), and it was found with the constants,  $c = 161.8$ ,  $a = 0.667$  and,  $b = 0.0883$ ; between 4.2° K and 1.4° K,  $\Delta T/T \approx 1$  per cent and below 1.4° K,  $\Delta T/T \leq 1$  per cent. The results are illustrated in figures 3 and 4.

### 3.6 Tunneling Sample Preparation

The Al - Al<sub>2</sub> O<sub>3</sub> - Pb tunneling sandwiches in this experiment, were prepared in an Edwards multi-filament vacuum coating unit, model 12E3, with an ultimate vacuum of 10<sup>-6</sup> torr. All evaporations were done at about 2 x 10<sup>-5</sup> torr. The films were deposited onto a substrate of a flame polished microscope slide section, approximately 0.5" square. Initially, the substrate was cleaned in a soap solution in an ultrasonic cleaner for about 10 minutes, making certain that there was no residual grease or grime remaining. The slide was then

cleaned for another three to five minutes in isopropyl alcohol. Distilled water was used in thoroughly rinsing the substrate, then dried with lint free tissues (Kimwipes). Immediately upon drying, the substrate was transferred to the evaporator.

The substrate was placed in a holder mounted twelve inches directly above the filament, from which the evaporation was to take place. The holder contained the mask, which was designed such that a pair of tunneling junctions were prepared simultaneously. Both of the evaporated strips of aluminum and lead were in the shape of a dumbbell to facilitate the attachment of electrical leads, with two aluminum strips perpendicular to the lead strip and separated by aluminum oxide. These strips were 0.005" wide, the ends 0.031" in diameter, and the overall length was 0.32".

The film thickness was monitored by a 6 Mhz. crystal oscillator, the crystal mounted slightly above the substrate holder, and the frequency monitored by a Hewlett Packard model 3734A frequency counter. For this geometry of crystal substrate and filament, it had been determined<sup>2</sup> that to a very good approximation in a 200 Khz. range; for aluminum, a deposition rate of  $1 \text{ \AA}/\text{sec}$ . corresponded to a decrease of frequency of 1 Hz./sec. For lead, the same deposition rate corresponded to a decrease of frequency of 5 Hz./sec.

The filament for evaporating the aluminum consisted of a coil 0.22" in dia., containing 6 loops made from 3 twisted strands of 0.02" dia. tungsten wire.

<sup>2</sup> Previously determined by R. C. Dynes, McMaster University, 1965.

The aluminum, in the form of 0.06" dia. wire (Cominco 99.9995 per cent pure) was cut into 0.5" segments, which were bent into a hairpin shape and hung from alternate loops. The aluminum evaporates from the wetted tungsten filament with no danger of tungsten contamination. The filament for evaporating lead consisted of an molybdenum boat, in which the lead (Cominco 99.9999 per cent pure) was initially stripped of its oxide and placed in the boat.

After evaporation of the aluminum strips, air was allowed into the evaporator for a pre-determined time, in order to form the oxide. This time varied, according to the temperature and humidity of the air. The mask was then changed, and the lead strip evaporated at right angles to the aluminum strips. The thickness of the oxide was not measured directly, but estimated from electrical resistance measurements at room temperature to be about  $20 \text{ \AA}$  thick. The completed sample was then mounted on the copper bottom of the helium-3 pot previously described, and electrical leads were attached to it, with the aid of indium solder. It was found that indium solder made a good electrical contact with the films, and adhered well, even at helium-3 temperatures.

The tunneling barrier increased in thickness due to oxide growth, such that the electrical resistance of these tunnel junctions were of the order 100 ohms by the time the exchange gas chamber previously described was evacuated. This evacuation was necessary in order to prevent further oxide growth; hence, preserving the sample to such a time in which the experiment was to be performed. It was found that if these tunnel junctions were left at atmospheric pressure for a period of twenty-four hours, the barrier resistance increased by several orders

of magnitude, corresponding to a barrier which was impenetrable.

### 3.7 Current vs Voltage Measurements

The hybrid block diagram-circuit schematic, used in obtaining the I-V characteristics of the tunneling junctions, is as shown in figure 5. D-C bias for the junction is provided by a Harrison model 6200A programmable power supply. The output voltage is programmed by a Philips model PM5168 function generator, operated in the positive sawtooth output mode and the frequency continuously variable. A typical sweep speed used was about 1 mv./minute.

With the resistance  $R_2$  at zero, the source impedance, as seen by the tunneling junction, is essentially  $R_4$ , which is always kept much less than the static resistance  $R_s$  of the tunneling sample, typically about 100 ohms. This ensures that the tunneling junction always sees a constant voltage source, which is necessary for suitable plotting of the I-V characteristics. This is true whenever the value of the current measuring resistance  $R_5$  is such that  $R_4 < R_5 < R_s$ .

The sample in the form of a four terminal network, eliminates errors in voltage measurements, in which the voltage developed across the insulating barrier, is measured from the two terminals of the sample not included in the main current path. This measured voltage is then fed into the X input of a Moseley model 7030A X-Y recorder. The tunneling currents are obtained from measurements of the voltage drop across the current measuring resistor  $R_5$ . This resistor is a selected standard resistor accurate to  $\pm 1$  per cent. This d-c signal across  $R_5$  is fed into the Y input of the X-Y recorder. Impedance

and signal levels are such that intermediate buffer amplifiers are not required.

### 3.8 Derivatives of the I-V Characteristics

As was discussed in Chapter 2.4, a particularly convenient method of determining the width of the energy gap of a superconductor, is by obtaining the points of inflection on the I-V characteristic. This is accurately determined by obtaining the first derivative of the I-V characteristic.

If we consider the application of a sinusoidal modulating voltage  $e_o \cos wt$ , such that the excursions of voltage swing about the bias voltage  $V_o$  are extremely small, the current tunneling through the barrier can be expanded as a function of the voltage. The Taylor expansion about the arbitrary reference bias voltage  $V_o$  is,

$$I(V_o + e_o \cos wt) = I(V_o) + \left. \frac{dI}{dV} \right|_{V_o} (e_o \cos wt) + \text{2nd and terms of higher order.}$$

The second and higher order terms of the series are omitted, since at the small fundamental signal levels used, and the choice of the circuit parameters used, are such that the contribution of these terms to the first term are small, and can be neglected. Hence, to a very good approximation, the first derivative, or the dynamic a-c conductance, is obtained. Therefore, with a suitable modulation voltage applied to the tunneling junction the  $\frac{dI}{dV}$  function may be easily obtained at a given reference voltage  $V_o$ . In addition, if this reference voltage is made to be linearly and slowly time varying, then the  $\frac{dI}{dV}$  function may be obtained over the entire region of bias interest.

The hybrid schematic used in plotting this derivative is illustrated in figure 6. The General Radio audio oscillator supplies a 1 Khz. sinusoidal signal with very little distortion. The frequency was chosen because of the practical convenience of it, and the frequency is high enough that it will not affect the slow d-c sweep. This modulation is inserted into the circuit across  $R_4$  so that the small modulation superimposed on the larger d-c sweep voltage will be seen by the sample. The amplitude of this modulation must be small, relative to the detail on the curve which is to be investigated. If the modulation is of the same order as the detail, the modulating signal will smear the sharpness of the detail.

If the d-c sweep is fast or "jerky", and of the same rate as the modulating signal sweep, the harmonics of the 1 Khz. produced will not be a true indication of the non-linearity of the tunneling junction, but will also be a function of the sweep speed. These problems are overcome by the use of the Philips variable speed function generator driving the bias supply. A typical sweep speed used in this experiment was about 1 mv./minute. This sweep speed does not in any visible way affect the resultant harmonics of the modulating signal.

For the measurements of the energy gap, an a-c probe of about 100  $\mu$ v p-p seemed to be adequate to determine the derivative of the curve, without appreciable smearing. This was determined by observing the shift of the  $\frac{dI}{dV}$  vs. V characteristics as a function of modulating voltage. Once no shift was observed, the modulation voltage was reduced to one half that value.

The major problem confronting this method of obtaining the derivative is

that of suppressing the noise, and allowing the "pure" signal to be filtered through. Across the current measuring resistor  $R_5$ , there is a Keithley 1034 transformer, which is connected to the input of a sharply tuned 1 Khz. amplifier. From this instrument, the amplified signal is fed into a Princeton Applied Research Model JB-4 lock-in amplifier, which filters, amplifies, and detects the 1 Khz. signal, giving a d-c output proportional to the signal detected. From this detector, the d-c signal is fed into the Y input of an X-Y recorder, thus giving the desired derivative as a function of applied voltage  $V$ . By adjusting the output filter on the lock-in amplifier and varying the sweep speed of the power supply accordingly, the noise level can be reduced without appreciably altering the resolution of the detection system.

It is also necessary to supply to this lock-in amplifier a reference signal which has the same frequency as, and at the same phase as, the signal under observation. This is achieved by amplifying the small modulation voltage by a Dymec 2460-A amplifier, and this signal is fed into the reference terminals of the lock-in amplifier. The incoming signal phase is adjusted on the lock-in amplifier.

### 3.9 Transition Temperature Measurement

Among the techniques of transition temperature measurement, the simplest is to measure the temperature at which the d-c resistance of the film vanishes. However, there is an objection to using this method, and that is, for most films, the edges are not sharply defined. As a result, the thin edges of the

film exhibit an enhanced transition temperature. Once the thin edges of the film pass into the superconducting state, zero resistance is measured, and it is no longer possible to measure the bulk  $T_c$ .

A much more reliable technique is to measure the temperature at which the current voltage characteristic exhibits the vanishing of the energy gap as the metal passes from the superconducting, to the normal state. For the case of multiple gaps, due to the thin edges of the films, this technique presents no difficulties, since the largest bump on the I-V characteristics corresponds to the bulk tunneling of the metal, and will vanish at the lowest of the transition temperatures. However, for tunneling sandwiches, in which a thin film of aluminum is on one side of the barrier, and on the other side a thick aluminum film, multiple gaps present a problem, and that is, one cannot distinguish between the energy gap of the thin film, and those of the thin edges of the bulk film. This problem can be eliminated when the bulk aluminum film is replaced by lead. For some unknown reason, Al-Al<sub>2</sub>O<sub>3</sub>-Pb films do not exhibit multiple energy gaps.

## IV. RESULTS AND DISCUSSION

### 4.1 Thick Aluminum Films

The first work was conducted on thick (1000 - 2000 Å) Al-Al<sub>2</sub>O<sub>3</sub>-Al films on both sides of the oxide layer. The BCS gap parameter  $2\Delta(0)/kT_c$  showed large scatter and did not agree particularly well with the BCS prediction of 3.52 for a weakly coupled superconductor. Multiple energy gaps were observed in the I-V characteristics; however, these gaps did not affect the measurements. The chief difficulty with the Al-Al<sub>2</sub>O<sub>3</sub>-Al junctions was the lack of sharpness in the kink of the I-V curves, making it difficult to identify the energy gaps. Junctions having a different superconductor on the two sides of the oxide layer, exhibit a negative resistance region, not found in the Al-Al<sub>2</sub>O<sub>3</sub>-Al type junctions. This produces I-V curves with sharply defined features and allows a more precise determination of the energy gap.

Al-Al<sub>2</sub>O<sub>3</sub>-Pb junctions were prepared and found to give excellent results. No multiple energy gaps were observed, and the I-V characteristics were sharply defined. Figure 9 shows the temperature dependent energy gap as a function of temperature for an Al-Al<sub>2</sub>O<sub>3</sub>-Pb junction. The approximate thicknesses of the aluminum and lead films were 1500 Å. The solid curve in the figure represents the BCS temperature dependent energy gap as a function of temperature. The experimental points are indicated by points. The fit is quite good, and certainly

within the estimated experimental error  $\sim 1$  per cent. From the relation (T2),

$$\Delta(0) = \Delta(T) (1 - (T/T_c)^4)^{1/2}$$

where  $\Delta(0)$  is the energy gap at  $0^\circ\text{K}$ ; when  $T \approx 1/3 T_c$ ,  $\Delta(0) \approx \Delta(T)$  to a very good approximation. As it is the case in figure 9,  $\Delta(0) \approx 0.178$  meV and the transition temperature  $T_c = 1.17^\circ\text{K}$ , hence

$$2 \Delta(0) = 3.53kT_c$$

expressed in terms of  $kT_c$ . This value is in excellent agreement with that of Blackford and March (B4), whose extensive work on aluminum films indicate that the mean value of the BCS gap parameter is 3.53 with an r. m. s. deviation of  $\pm 0.02$ . No energy gap nor transition temperature enhancement was observed.

#### 4.2 Thin Aluminum Films

Upon obtaining satisfactory results with thick aluminum films, very thin ( $35-80 \text{ \AA}$ ) aluminum films were investigated. At first, (100-20-1500  $\text{ \AA}$ ), Al-Al<sub>2</sub>O<sub>3</sub>-Al junctions were prepared and investigated. As previously mentioned in Chapter 3.9, multiple energy gaps were observed, and presented a problem. The problem was, on the I-V curves one could not distinguish between the energy gap of the thin aluminum film, and those of the thin edges of the bulk aluminum film on the other side of the barrier. This problem was overcome by preparing (100-20-1500  $\text{ \AA}$ ) Al-Al<sub>2</sub>O<sub>3</sub>-Pb junctions. For some unknown reason, these junctions did not exhibit multiple energy gaps.

Figure 7 shows an experimental plot of current vs. voltage for an Al-Al<sub>2</sub>O<sub>3</sub>-Pb junction measured at  $1.07^\circ\text{K}$ , with the applied voltage extending

from 0 to approximately 3 millivolts. The thickness of the aluminum film is approximately  $100 \text{ \AA}$ , and that of the lead film  $1500 \text{ \AA}$ . Figure 8 illustrates the corresponding conductance vs. voltage characteristic at  $1.07^\circ \text{K}$ . It is noted that the characteristic is sharply defined with no evidence of multiple energy gaps present. Figure 10 illustrates the temperature dependent energy gap as a function of temperature for four Al-Al<sub>2</sub>O<sub>3</sub>-Pb junctions, having approximate thicknesses (35-80  $\text{\AA}$ ), and in all four cases,  $1500 \text{ \AA}$  of lead. Once again, the solid curve represents the BCS temperature dependent energy gap as a function of temperature. The experimental points are in good agreement with the BCS curve. The experimental results are summarized in Table 1.

In addition, an Al-Al<sub>2</sub>O<sub>3</sub>-Pb junction was prepared in which the aluminum film was formed by evaporating aluminum from a tungsten filament with an alumina insert, sample C of Table 1. The thickness of the aluminum film was approximately  $350 \text{ \AA}$  and exhibited an enhanced  $T_c$  close to that observed by Cohen and Abeles (C2). The enhanced  $T_c$  is of the same order of magnitude as those obtained on thin aluminum films, prepared in the absence of an internal supply of oxygen.

#### 4.3 Summary of Results

In all Al-Al<sub>2</sub>O<sub>3</sub>-Pb junctions prepared, no multiple energy gaps were observed in the conductance vs. voltage characteristics. Furthermore, the transition temperature  $T_c$ , of the thin aluminum films determined by the vanishing of the electrical d-c resistance, agreed with those obtained by the vanishing of the

energy gap, indicating no surface superconductivity in these films. Also, since all films were prepared in the same manner and approximately at the same deposition rate, about  $50 \text{ \AA}/\text{sec.}$ , there was no reason to suspect oxide or other contamination, above the level found in the thicker films, which showed no enhancements. The observed enhanced transition temperatures as well as the enhanced energy gaps of these thin films, were reproducible when the junctions were kept in a vacuum; however, at atmospheric pressure for a period of twenty-four hours, the oxide layer grew to such a thickness, that the layer was impenetrable.

An electron micrograph was obtained of an aluminum film approximately  $100 \text{ \AA}$  thick. It was noted that there was an extremely wide range of crystallite sizes, with unusually large separations between the crystallites. An electron diffraction pattern contained rings characteristic of aluminum and no extra rings corresponding to impurities were detected. Furthermore, an electron micrograph was obtained of an aluminum film approximately  $300 \text{ \AA}$  thick, prepared by evaporation from a tungsten filament with an alumina insert. This micrograph appeared to be no different than that of the  $100 \text{ \AA}$  film which was prepared by evaporation from a wetted tungsten filament.

## V. MECHANISMS OF ENHANCEMENT $T_c$

### 5.1 Quantization of Electronic Motion

Parmenter (P1) has calculated the enhancement of  $T_c$  for a granular superconductor, due to the quantization of electron motion. Starting from a simple model; a system composed of many microscopic grains of superconductor as cubes of equal size of length  $a$ , all stacked side by side without gaps, separated by an insulating layer  $d \ll a$  being thin enough to allow tunneling by Cooper pairs of electrons, Parmenter found that the enhancement could be described by an increased electron-phonon interaction. The author determined that deviations from the BCS predications occur, and are significant when the grain sizes become comparable with a characteristic length  $L = (\lambda_f^2 \xi_0)^{1/3}$ , where  $\lambda_f$  is the Fermi wavelength and  $\xi_0$  the Pippard coherence length in a pure metal at  $T = 0^\circ \text{K}$ . For aluminum,  $L$  corresponds to  $62 \text{ \AA}$ . Furthermore, Parmenter found that there was an enhancement of the energy gap  $\Delta(0)$ , which increased faster than  $T_c$ , so that when  $a \ll L$ , the ration  $2 \Delta(0)/kT_c$  increased from the usual BCS value of 3.528.

Although Parmenter's idealized model is able to account qualitatively for the observed enhancement of  $T_c$ , it is apparent that the model cannot be applied to the crystalline films prepared by the low-temperature deposition technique, or by the preparation in an oxygen atmosphere, or by the technique described here. In all of these films, there is a wide distribution of grain sizes, as well

as large regions in which the crystallites are not completely separated. On the basis of Parmenter's model, the distribution of grain sizes is expected to result in a corresponding distribution in energy gaps. The tunneling characteristics observed are extremely sharp, and there is no evidence of multiple energy gaps. Walmsley et al (W1), have pointed out that the energy gap variations will be averaged out if there is no variation of film texture over a tunneling area equal to the coherence distance of the film. They estimated that this distance is of the order four times the film thickness at  $T = 1.17^{\circ} \text{K}$ . An electron micrograph of an aluminum film approximately  $100 \text{ \AA}$  thick, and of the same order as that reported by Walmsley et al, shows that there is a significant variation of crystallite sizes within this coherence distance. Moreover, no observed increase was found in the ratio  $2 \Delta(0)/kT_c$ , as predicted by Parmenter.

Blatt and Thompson (B5) have investigated by calculation the pairing of electrons in a thin film. Starting from pair wavefunctions similar to those used by Anderson (A2) in his theory of dirty superconductors, periodic boundary conditions were imposed on the wavefunctions, and a solution was obtained by Thompson and Blatt (T1) by considering the Schrodinger equation in one dimension with a constant potential. An interesting feature of the energy gap solution is that it contains a number of sharply pronounced resonances, which depend upon the boundary conditions imposed on the wavefunctions. The amplitude of these resonances are related to the pairing energy, and increases as the film thickness decreases, which leads to enhancement values which are almost always higher than the bulk values.

The model is an oversimplified one, as well as unrealistic, furthermore, one-dimensional superconductivity has been shown an impossibility by Ferrell (F1).

Because of the incomplete isolation of individual crystallites, Cohen and Abeles (C2) have pointed out that any model based on the quantization of electronic motion, breaks down. The discrete energy levels of the crystallites form bands, and when the width of these bands near the Fermi level becomes of the order of the spacing between bands, the models break down. They have shown that these models are not applicable to their films.

## 5.2 Surface Enhancement

It has been proposed by Cohen et al (C1), that electrons can form Cooper pairs across the insulating layer in a superconducting sandwich for all choices of metals on both sides of the insulating barrier. In this theory, a Cooper pair is formed from an electron on one side of the sandwich, with an electron on the other side of the barrier. The attractive electron-phonon interaction is weakened by the barrier; however, it has the effect of greatly reducing, and even changing, the sign of the Coulomb interaction. Hence, the effective electron-phonon attraction for these Cooper pairs can be larger than that for pairing on the same side of the barrier, resulting in enhanced  $T_c$ 's. According to the theory the electron pairing is confined to a layer of depth  $d \sim$  several hundred angstroms on either side of the insulating layer, and in thin films  $\lesssim d$ , the pairing is uniform throughout the film. If a superconducting sandwich is prepared such that

thin parallel films  $\lesssim d$ , separated by a thin oxide layer, and a supercurrent is made to flow in one of the films; pairing across the barrier exists if a corresponding supercurrent is measured in the other film.

Such an aluminum sandwich  $\approx 100 \text{ \AA}$  was constructed, separated by an oxide layer  $\approx 20 \text{ \AA}$ , and a supercurrent of  $1.5 \mu\text{A}$  was made to flow in one of the films. A Keithley electrometer was placed across the other film, and no corresponding current flow was observed on the lowest scale ( $10^{-12}$  ampere scale). In all fairness, this one experiment certainly does not invalidate the theory of electron pairing across the barrier. However, it does suggest that no such pairing exists. There is yet another objection to the above mechanism, and that is, it is unable to account for the enhancement observed in films prepared by evaporating metals onto cold substrates (B6, K2), nor to the enhancement observed in thin films deposited onto room temperature substrates, but not in the form of a tunnel junction.

Ginzburg (G2) has suggested that Cooper pairs can be formed in a layer of metal near to the surface of a superconductor-dielectric interface, as well as between electrons in surface states of the metal. The BCS theory of superconductivity remains valid for the two-dimensional case, and in particular the well known formula

$$kT_c = 1.14 \hbar\omega \exp(-1/N(O)V)$$

remains valid; however,  $N(O)$  and  $V$  are different for the two-dimensional case; hence, a corresponding change in  $T_c$ . Ginzburg mentions the possible mechanisms for this enhancement as "variation of screening length and the exchange by surface

phonons".

Experimentally, with surface superconductivity, one would expect to find two values of the energy gap: an energy gap resulting from the pairing in the bulk of the metal film, as well as an energy gap resulting from pairing in the surface regions. Two energy gaps were not observed experimentally in any of the tunneling curves. It, therefore, appears that this mechanism cannot explain the observed enhancement.

## CONCLUSIONS

It is thought that the enhancements observed to date arise in films which are basically the same. The difference between these films lies only in the method of preparation. The experimental evidence to date indicates that these films are essentially comprised of a system of very small crystallites, with a wide distribution of crystalline sizes. The stability of these enhanced superconducting systems depends largely on the method of preparation. Furthermore, the theories proposed to date inadequately explain the enhancements and cannot explain the decrease in  $T_c$  as the films are made thinner, as observed in the strong coupling superconductors Hg and Pb. It is evident that any theory based upon crystallite size alone cannot explain the enhancements. However, experimental data shows that the enhancements are a function of crystallite size, independent of film thickness. Hence, it is thought that for any theory to work, a new parameter, the volume density of crystallites must be introduced.

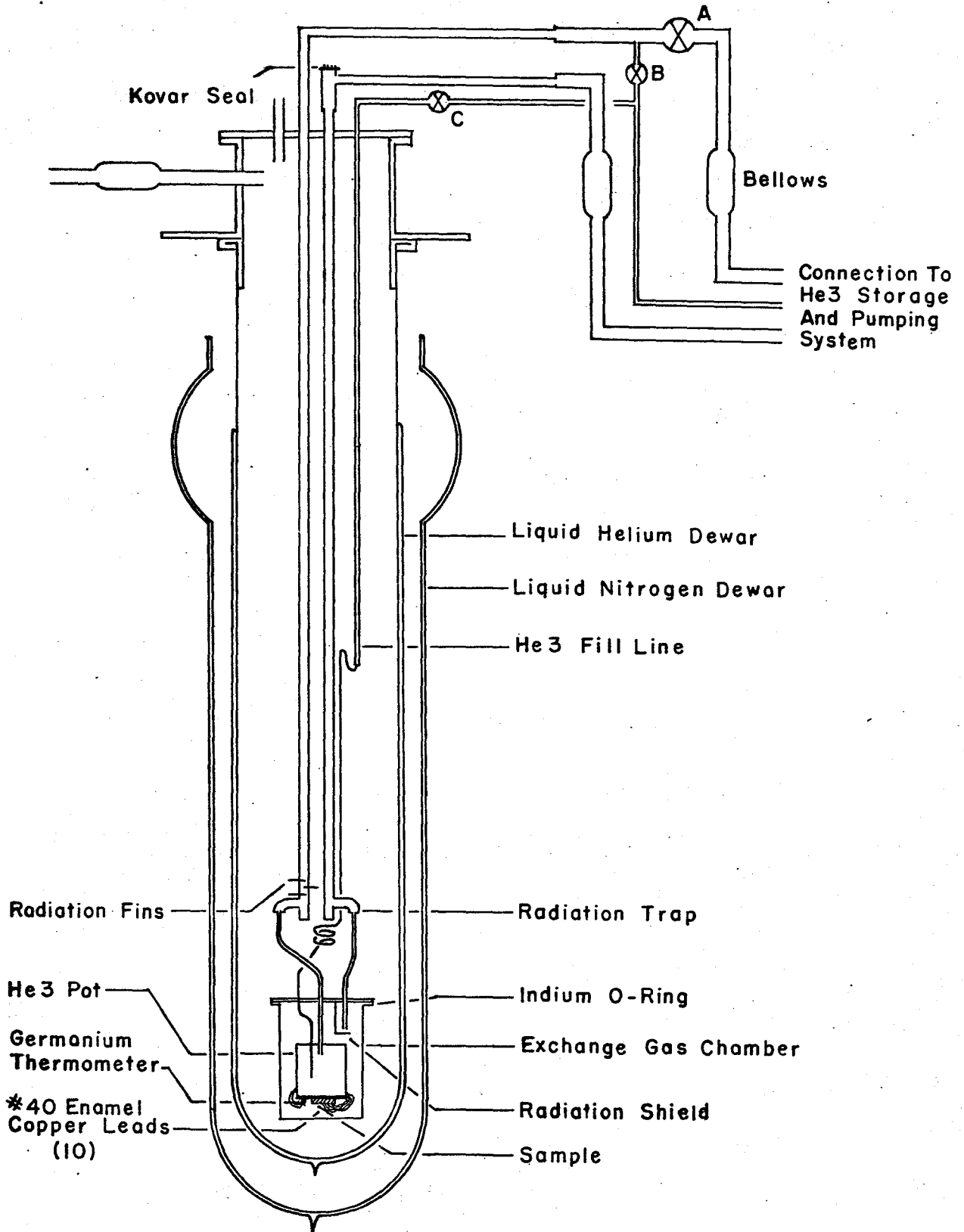


Figure 1

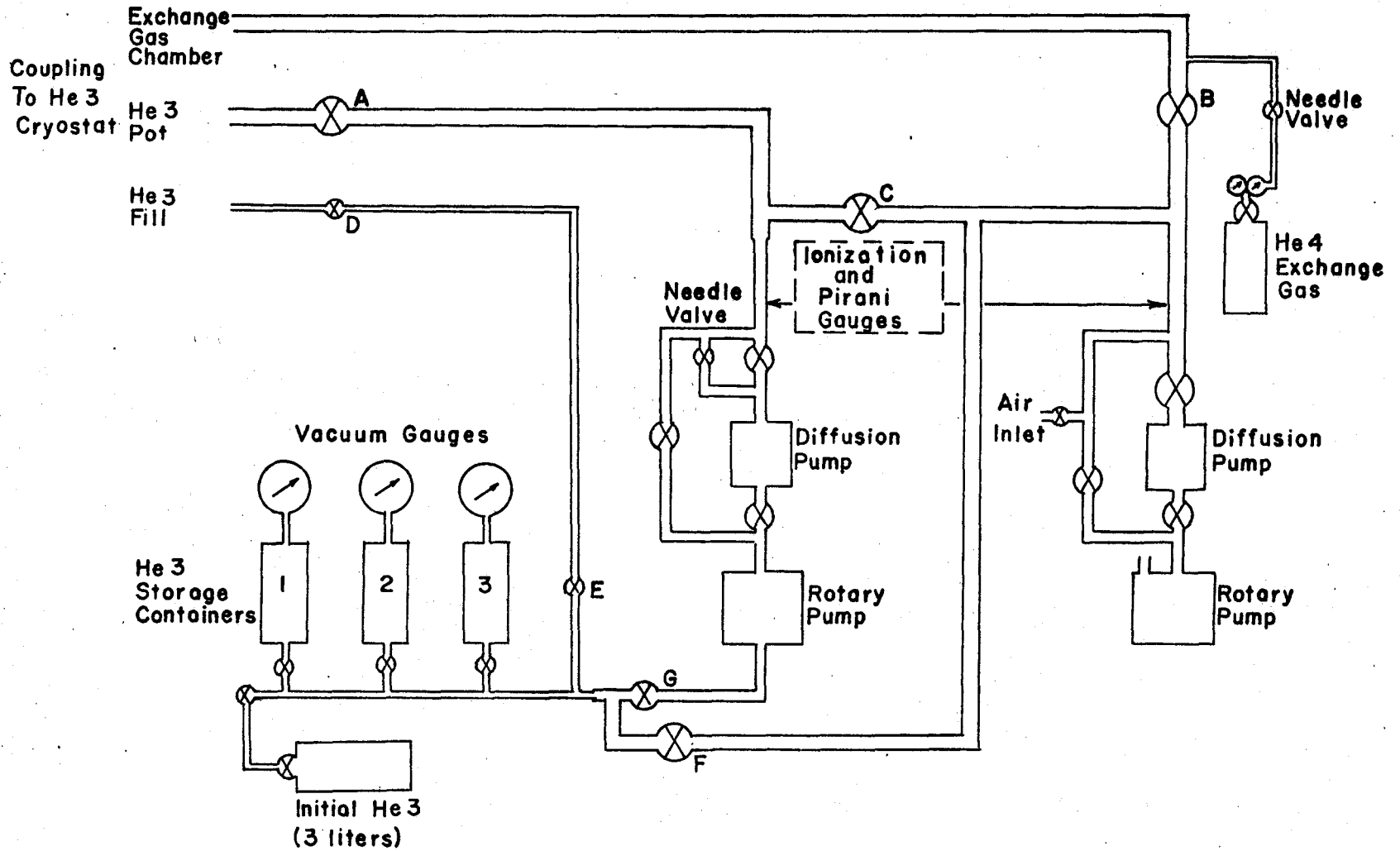


Figure 2

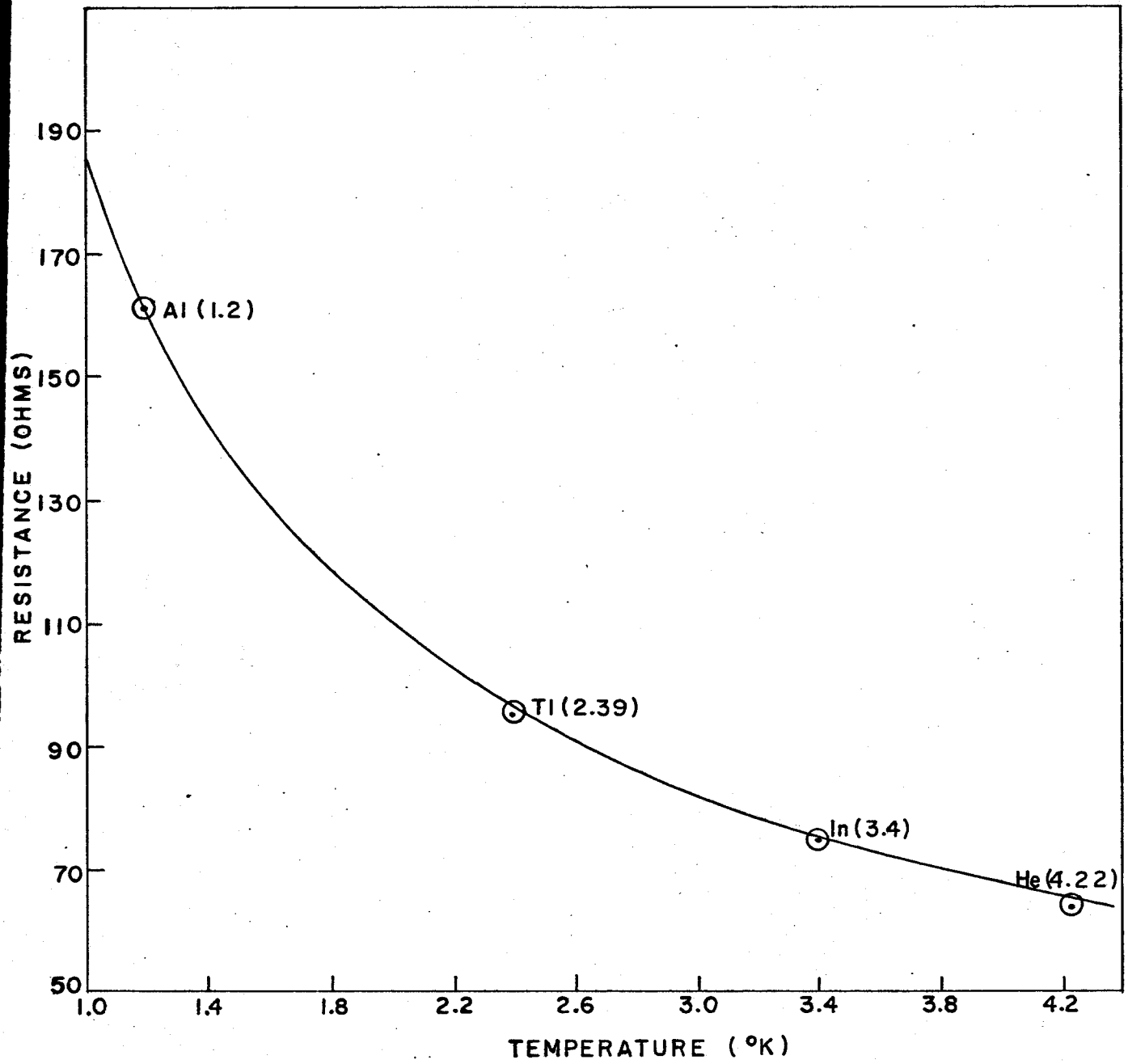


Figure 3

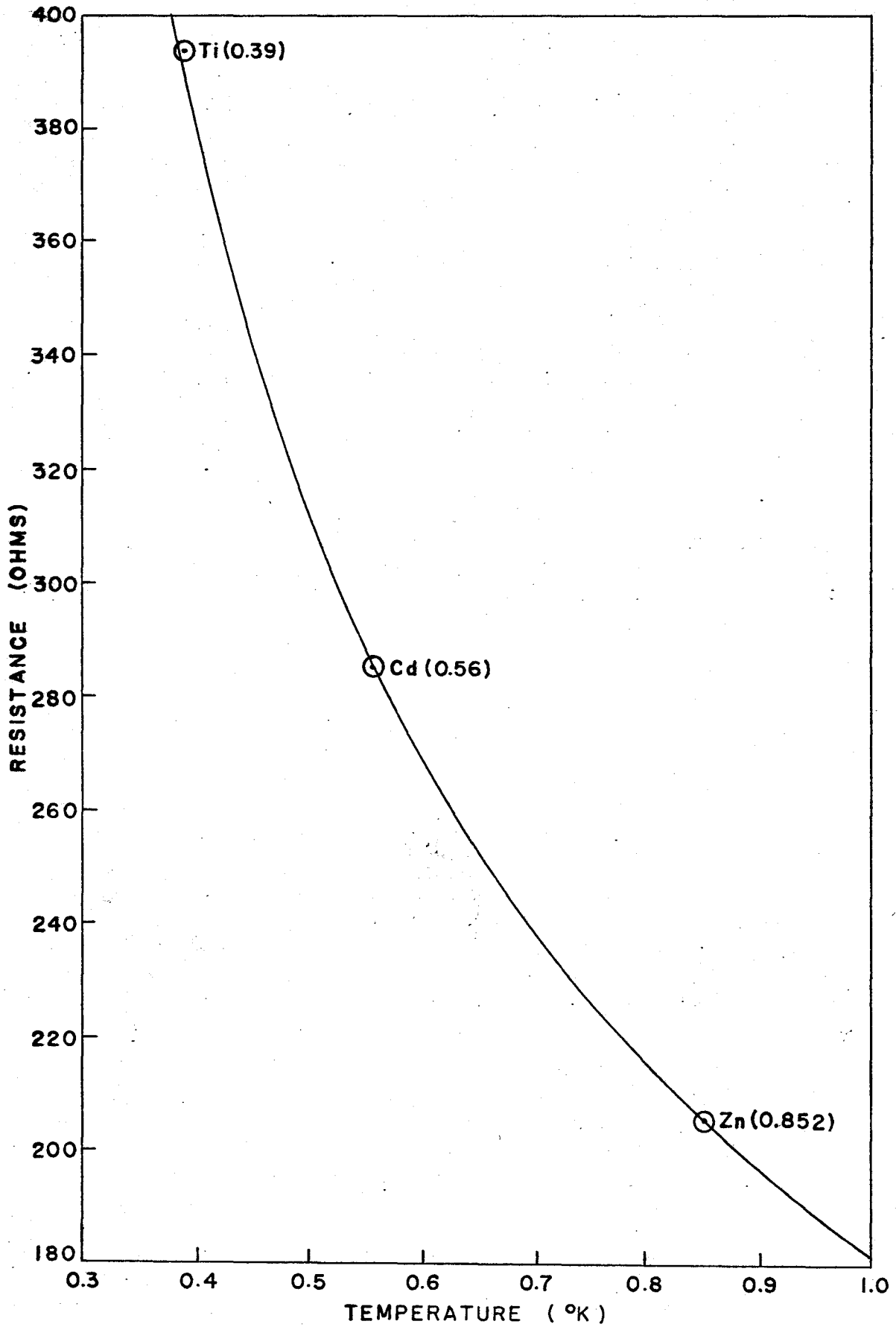


Figure 4

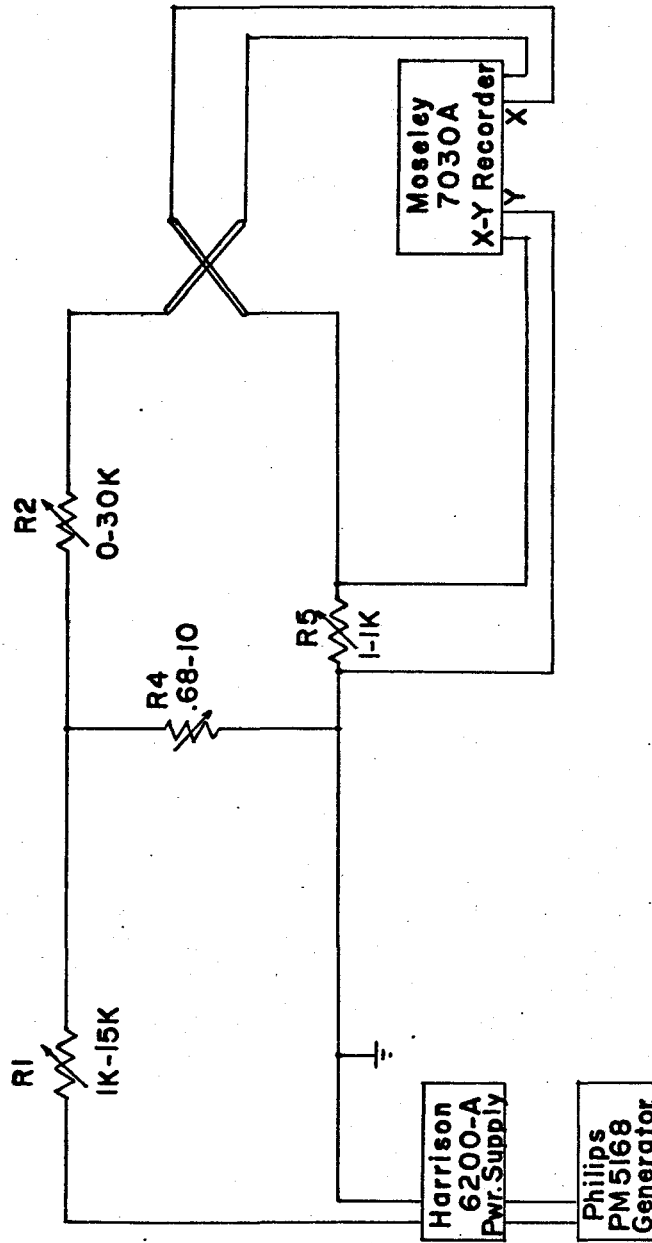


Figure 5

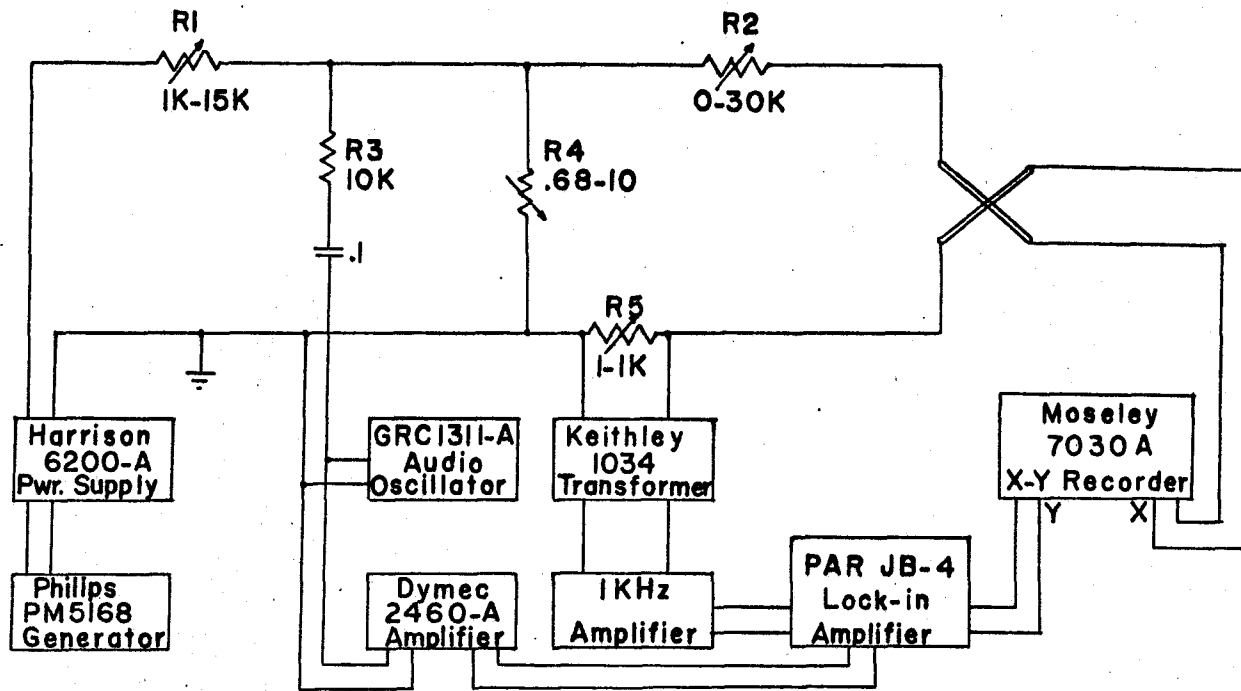


Figure 6

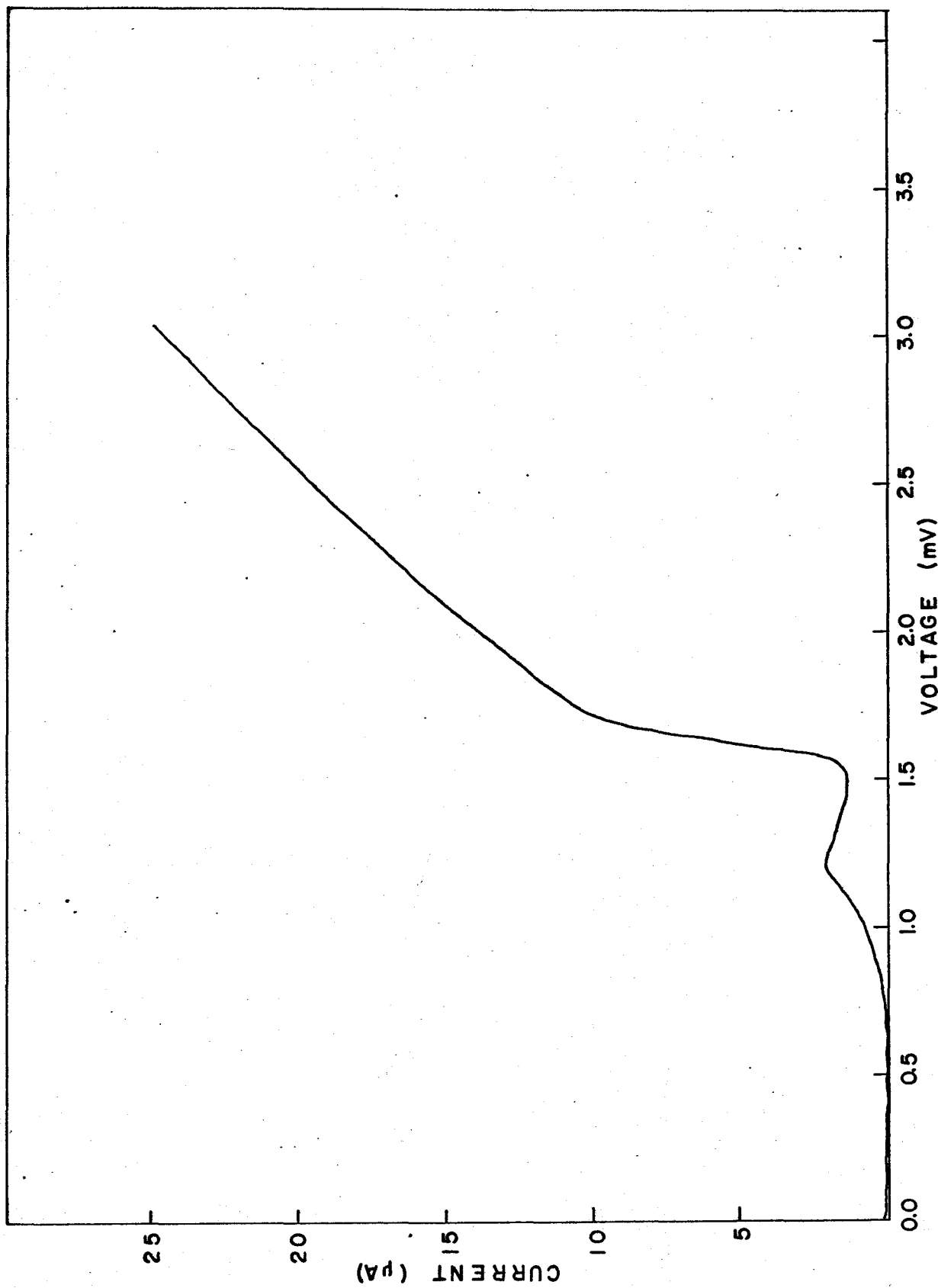


Figure 7

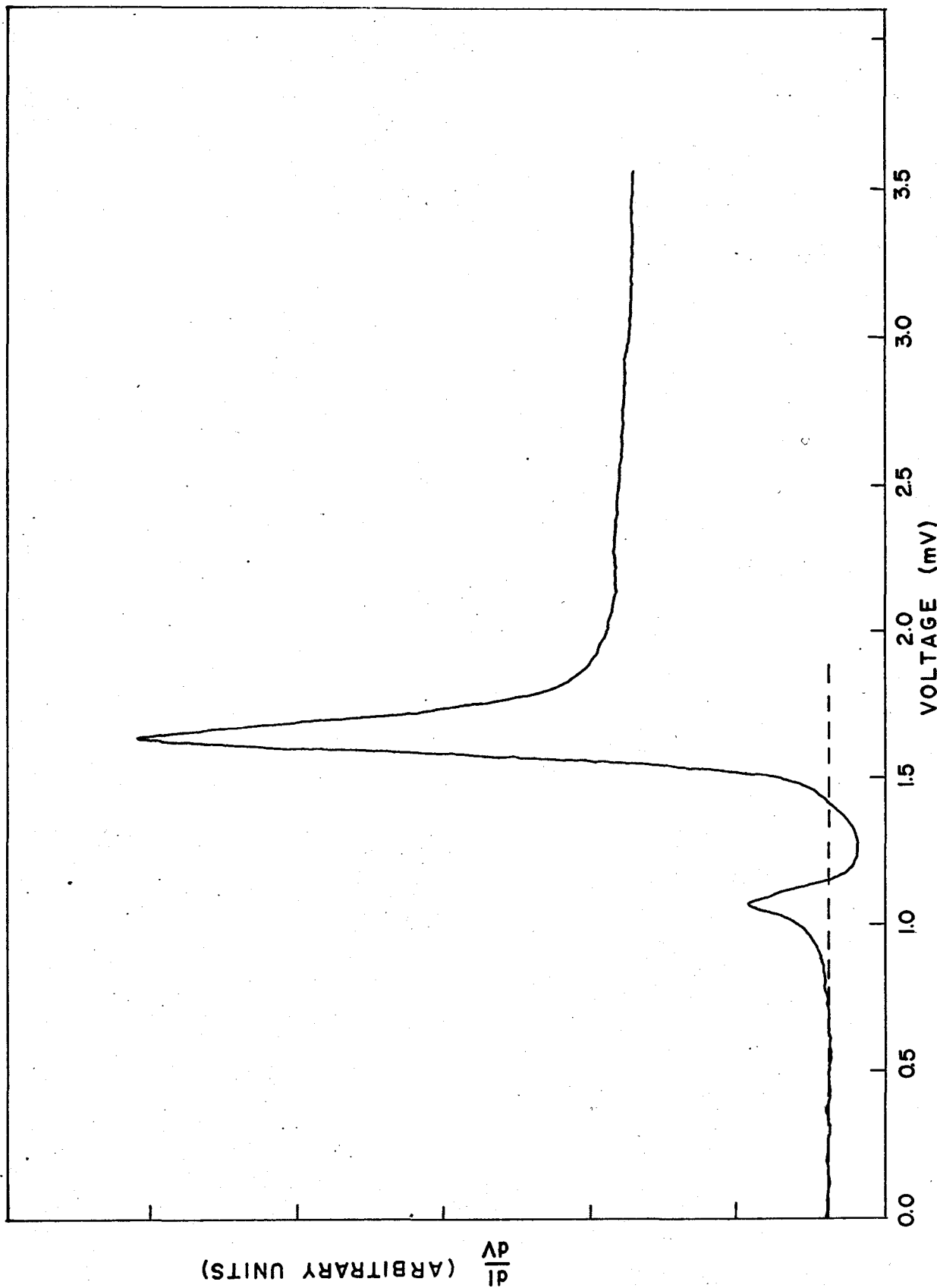


Figure 8

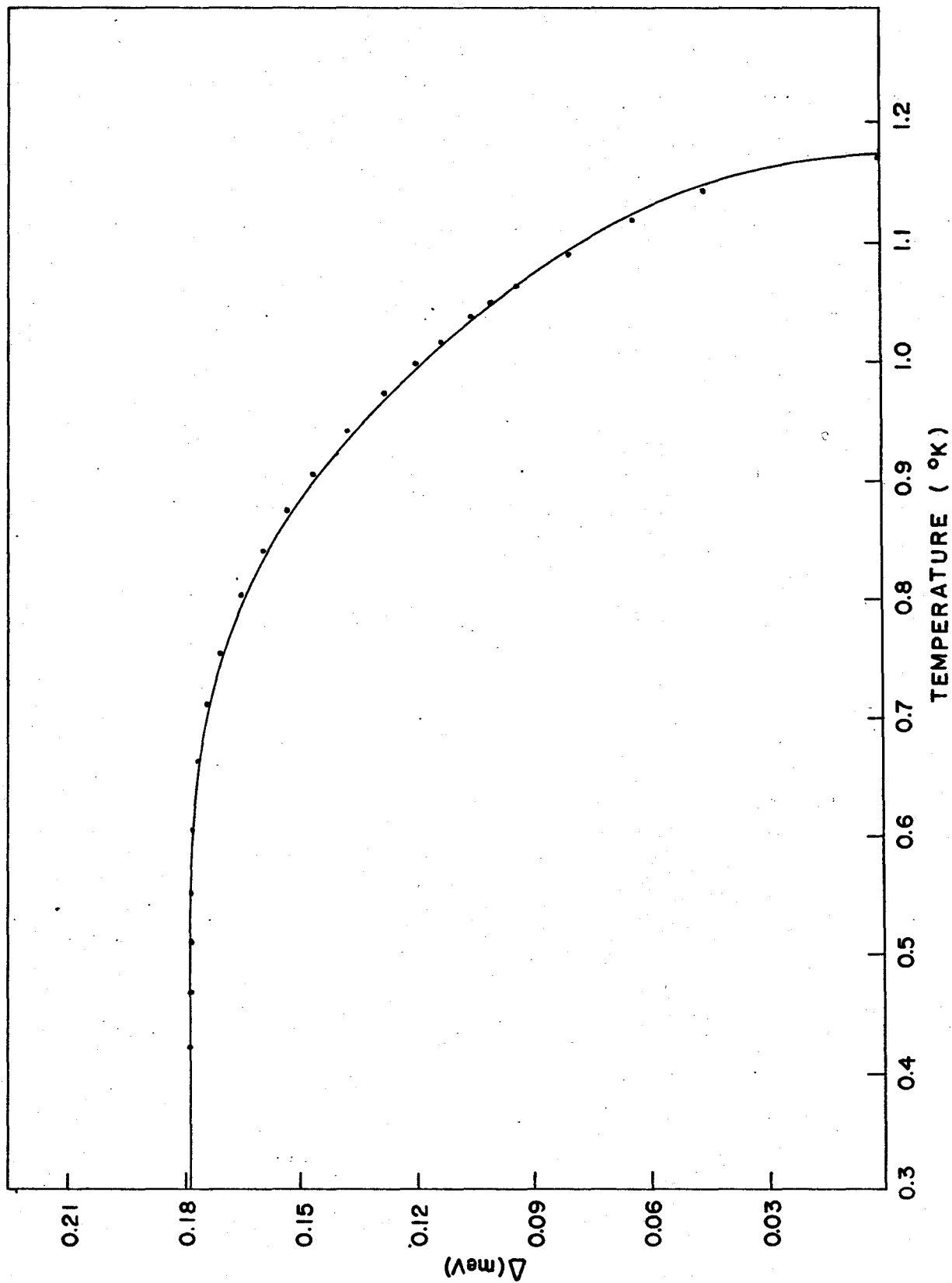


Figure 9

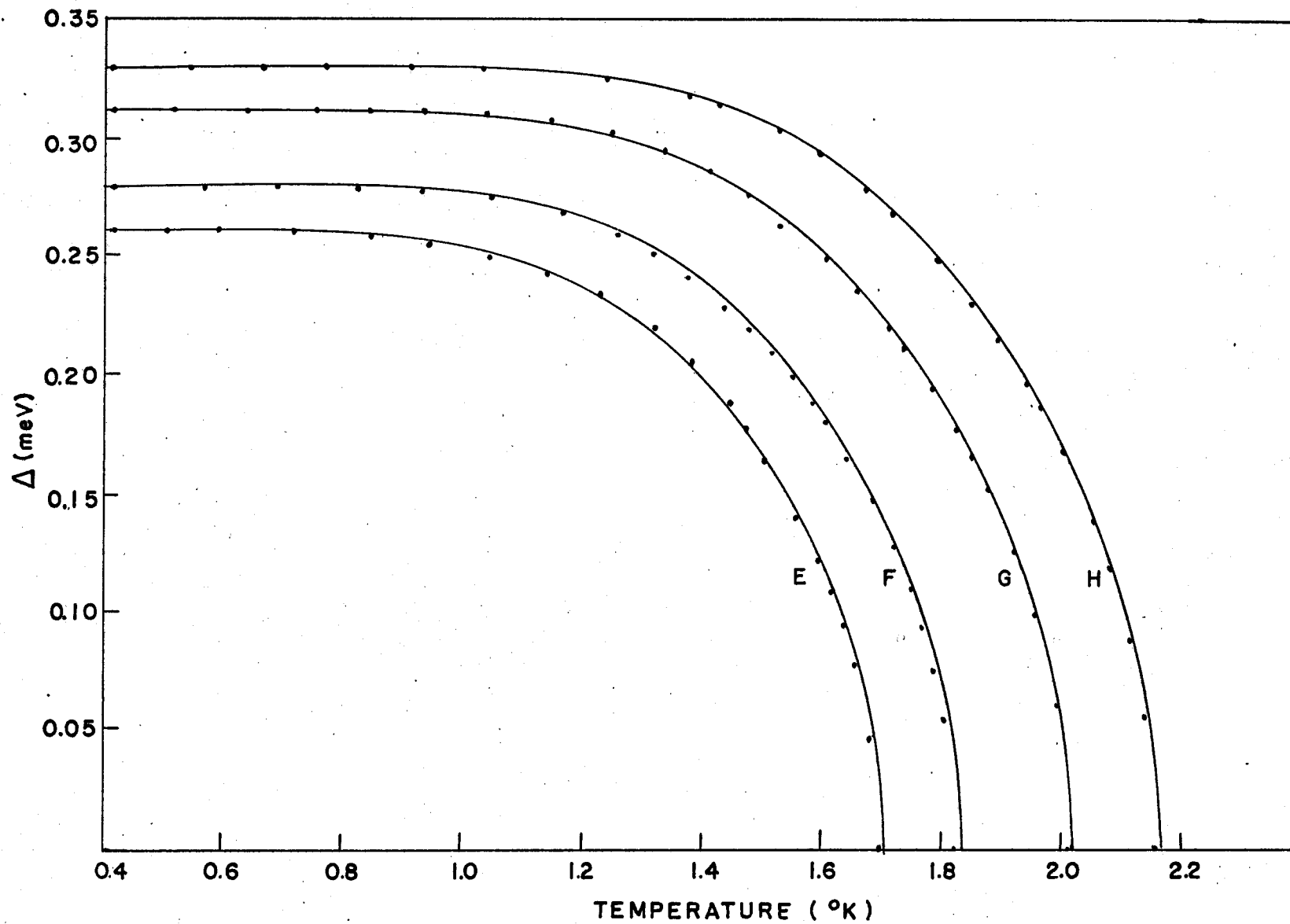


Figure 10

SAMPLE	d(A°)	T <sub>c</sub> (°K)	Δ(meV)	2Δ(0)/kT <sub>c</sub>
A	2000	1.18	0.180	3.54
B	1500	1.17	0.178	3.53
C*	350	1.96	0.298	3.53
D	100	1.67	0.256	3.56
E	80	1.70	0.260	3.55
F	70	1.83	0.280	3.55
G	50	2.05	0.313	3.54
H	35	2.16	0.330	3.54

\* Alumina insert

Table I

## BIBLIOGRAPHY

- A1** Abeles, B., Cohen, R.C., Cullen, G.W., Phys. Rev. Letters 17, 632 (1966).
- A2** Anderson, P.W., J. Phys. Chem. Solids 11, 26 (1959).
- B1** Bardeen, J., Phys. Rev. Letters 6, 57 (1961).
- B2** Bardeen, J., Cooper, L.N., Schrieffer, J.R., Phys. Rev. 108, 1175 (1957).
- B3** Bardeen, J., Pines, D., Phys. Rev. 99, 1140 (1955).
- B4** Blackford, B.L., March, R.H., Can. J. Phys. 46, 141 (1968).
- B5** Blatt, J.M., Thompson, C.J., Phys. Rev. Letters 10, 332 (1963).
- B6** Buckel, W., Hilsch, R., Z. Physik 138, 109 (1954).
- C1** Cohen, M.W., Douglass, Jr., D.H., Phys. Rev. Letters 19, 118 (1967).
- C2** Cohen, R.W., Abeles, B., Phys. Rev. 168, 444 (1968).
- C3** Cooper, L.N., Phys. Rev. 104, 1189 (1956).
- D1** DeBoer, J., Progress in Low Temperature Physics, Vol. 1, (North Holland, Amsterdam, 1955), pp. 397-402.
- F1** Ferrell, R.A., Phys. Rev. Letters 13, 330 (1964).
- G2** Ginzburg, V.L., Phys. Letters 13, 101 (1964).
- H1** Hammel, E.F., Progress in Low Temperature Physics, Vol. 1, (North Holland, Amsterdam, 1955), pp. 89-90.

- K1 Kammerer, O.F., Strongin, M., Phys. Letters, 17, 224 (1965).
- K2 Khukhareva, I.S., Soviet Phys. JETP 16, 828 (1963).
- P1 Parmenter, R.H., Phys. Rev. 167, 387 (1968).
- P2 Powell, R.L., Blanpied, W.A., Thermal Conductivity of Metals and Alloys at Low Temperatures (U.S. Government Printing, Washington, 1954), pp. 49-55.
- R1 Rose-Innes, A.C., Low Temperature Techniques (English Universities Press, London, 1964), p. 64.
- S1 Seidel, G., Keesom, P.H., Rev. Sci. Instr. 29, 606 (1958).
- S2 Strongin, M., Kammerer, O.F., Douglass, Jr., D.H., Cohen, M.H., Phys. Rev. Letters 17, 121 (1967).
- T1 Thompson, C.J., Blatt, J.M., Phys. Letters, 5, 6 (1963).
- T2 Tinkham, M., Low Temperature Physics (Cordon and Breach, New York, 1961), p. 177.
- W1 Walmsley, D.G., Campbell, C.K., Dynes, R.C., Can. J. Phys. 46, 1129 (1968).
- W2 Weast, R.C., Handbook of Chemistry and Physics, 46th Edition (The Chemical Rubber Co., Cleveland, Ohio, 1965-1966), pp. E67-68.
- Z1 Zemansky, M.W., Heat and Thermodynamics (McGraw Hill, New York, 1957), p. 355.